Centrifuge modelling of Dutch railway embankments on soft clays: the RESET experimental program

Cihan Cengiz[1*], *Cor* Zwanenburg[1], *Timo* Schweckendiek[1], *Alexander* van Duinen[1], *Mark* Post[1], *Agnes* van Uitert[2], *Stefano* Muraro[3], *Maryam* Hallaj[3], *Cristina* Jommi[3,4]

[1] Deltares, Delft, The Netherlands
[2] ProRail, Utrecht, The Netherlands
[3] Department of Geoscience and Engineering, Delft University of Technology, Delft, The Netherlands
[4] Department of Civil and Environmental Engineering, Politecnico di Milano, Milano, Italy

1 Introduction

In the Netherlands, railway embankments founded on soft clay are sensitive to progressive deformation and pore pressure development under increasing traffic demands. Within the Rail Embankment for Safe Expansion of Traffic (RESET) research programme, a centrifuge test series was conducted to generate a controlled experimental dataset describing embankment behaviour at failure conditions. Eight centrifuge tests were performed at 50g using a 1:50 scaling ratio. The testing -programme included systematic variation of clay undrained shear strength, embankment geometry, ditch presence, and loading rate. The clay foundation consisted of consolidated kaolin, and the embankment was constructed of dense sand. Loading was applied under displacement control using a rigid plate with rotational freedom to allow realistic load redistribution. The instrumentation programme combined global load–displacement measurements, total and pore water pressure monitoring, in-flight T-bar strength profiling, particle image velocimetry (PIV) for full-field deformation analysis, and post-test 3D surface scanning. The present contribution elaborates on the experimental configuration and principal observed response patterns, providing a benchmark dataset for future modelling and assessment studies.

The RESET centrifuge programme comprises eight heavily instrumented tests defining a controlled experimental parameter space. As illustrated in Figure 1, the testing programme matrix is structured along three principal axes. The primary axis governs foundation stiffness contrast, achieved through systematic variation of the clay undrained shear strength, which enables isolation of the influence of subsoil stiffness on peak resistance, strain localisation, and post-peak kinematic evolution. The second axis investigates loading rate under displacement-controlled conditions, which permits examination of shear-rate effects on pore pressure generation and strain development. The third axis isolates the geometric boundary condition associated with the presence of a ditch, which alters lateral confinement and thereby affects the formation and extent of the failure wedge. These axes establish a mechanism-oriented framework within which the transition from punching-dominated response to progressive wedge development can be examined.

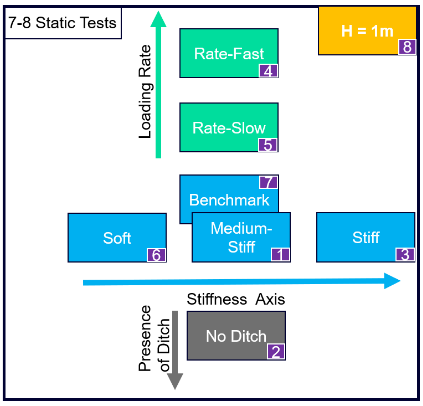

Figure 1. RESET centrifuge testing matrix structured along three principal research axes: foundation stiffness contrast, loading rate, and ditch presence.

2 Experimental configuration

All experiments were conducted in the Deltares GeoCentrifuge at a scaling ratio of 1:50 under a centrifugal acceleration of 50g. The model represents a typical Dutch railway embankment with a prototype height of 2.5 m founded on approximately 6 m of clay. A plane-strain half-embankment configuration was adopted within a rigid strongbox, with geometric proportions derived from representative field conditions. A detailed description of the experimental assembly, scaling considerations, and instrumentation layout is provided in [1, 2].

* Corresponding author: cihan.cengiz@deltares.nl

The clay foundation was prepared from Speswhite kaolin slurry and consolidated in-flight to predefined effective stress levels in order to achieve three target undrained shear strength ranges. The embankment was constructed of dense Baskarp sand using wet pluviation and controlled tamping to achieve high relative density. Foundation stiffness contrast was therefore governed by controlled variation of clay strength while maintaining comparable embankment properties.

Vertical loading was applied under displacement control using a rigid loading plate with rotational freedom, which enabled realistic load redistribution during deformation. The instrumentation programme comprised pore water pressure sensors, total stress cells, displacement transducers, in-flight T-bar penetrometer tests for strength verification, particle image velocimetry for full-field deformation analysis, and post-test three-dimensional surface scanning (Figure 2).

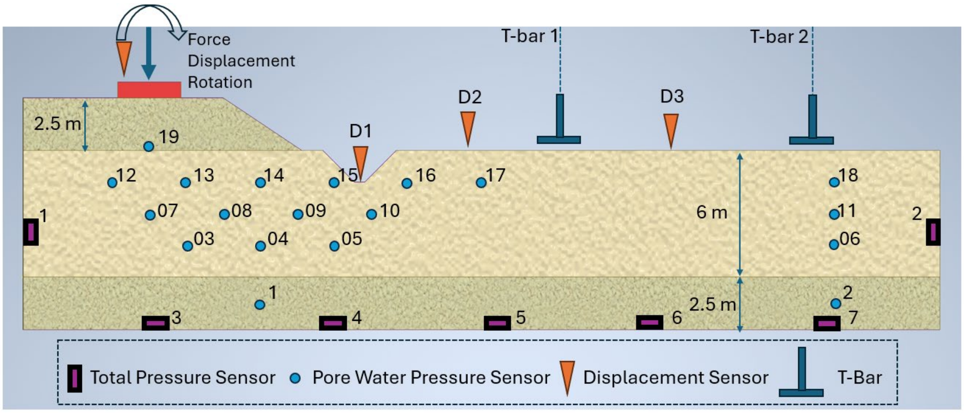

Figure 2. Instrumentation layout of the centrifuge model (adapted from Cengiz et al. [1]).

3 Foundation strength and embankment response

The experimental matrix incorporated three target undrained shear strength levels to systematically vary the stiffness contrast between the embankment and the clay foundation. The target strength states were achieved through controlled consolidation of Speswhite kaolin and were selected to represent soft, medium, and stiff foundation conditions. The strength profiles were defined using the SHANSEP framework (Stress History and Normalized Soil Engineering Properties). For the Speswhite kaolin used in the experiments, the SHANSEP parameters are $S_{uN} = 0.19$ and $m = 0.805$. Based on these parameters, three consolidation pressures of 64, 105, and 210 kPa were selected to achieve the desired undrained shear strengths of about 12, 20, and 40 kPa for soft, medium, and stiff clay, respectively. The one-dimensional coefficient of consolidation of the clay is on the order of $c_v \approx 1.5 \times 10^{-7}\ \mathrm{m}^2/\mathrm{s}$. The Speswhite kaolin had a liquid limit of 66%, a plastic limit of 27%, a plasticity index of 39%, and a specific gravity of 2.63.

To verify the target foundation strength conditions, a total of two in-flight T-bar penetration tests were performed during each centrifuge experiment. The diameter and length of the T-bar rod were 12 and 75 mm, respectively. The projected area of the T-bar is 900 mm^2 (or $9 \times 10^{-4}\ m^2$). With the 1 mm/s advancement rate, the loading is deemed to be undrained. A N_{kT} value of 10.5 was adopted to transform the penetration resistance into undrained shear strength [3].

Figure 3 illustrates the load-displacement curves obtained from the tests along with the measured tilt of the loading plates. The displacement axis in the plots is reported in prototype scale. Furthermore, Figure 4a presents the T-bar measurements acquired in-flight for all tests. Additionally, Figure 4b shows the relationship between the measured T-bar strength and the observed embankment resistance. The data indicate a clear correlation between foundation strength and peak load response, which confirms that the role of the stiffness contrast was successfully isolated. Lastly, Table 1 gives an account of the experimental parameters and the testing outcomes. The reference depth indicated in Table 1 refers to the mid-depth of the clay profile which corresponds to a model-scale depth of 60 mm. The peak embankment resistance refers to the maximum average pressure under the loading pad at early phases of loading and not to the spurious increase at the tail-end of the curves due to large deformations. The test involving the short embankment (Test 8) showed no distinct peak stress. Therefore, the mobilized strength at 100 mm prototype scale settlement is reported in Table 1. In general, the results indicate that the clay stiffness affects the embankment resistance and the measured peak resistance correlates well with the undrained shear strength of the clay profile. It is also seen that tilt accumulation in short embankments advance rapidly upon reaching large displacements. It should also be noted that the cosine of the tilt angle remained low within the displacement envelope where the peak resistance was recorded for all tests. In other words, up until a displacement value of 250 mm, no appreciable tilt is observed of the loading plate. Finally, Figure 5 illustrates the final failure geometry of an exemplar test alongside with the vector field of the displacements at a prototype scale displacement level of 500 mm.

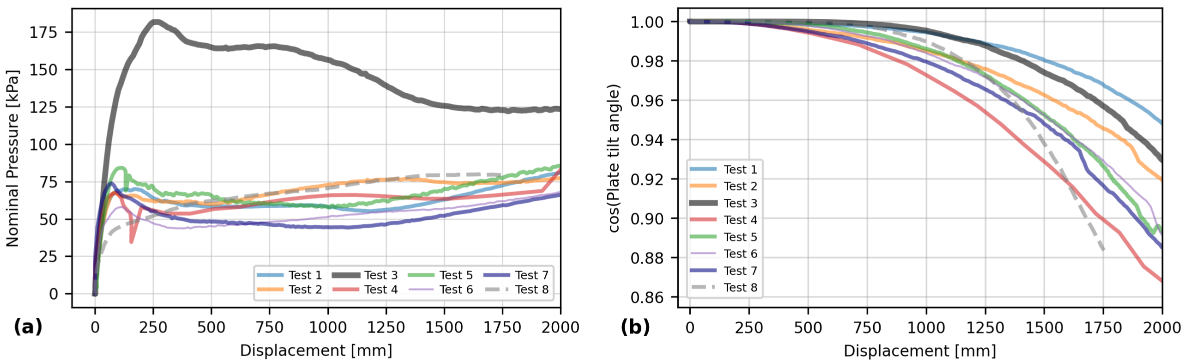

Figure 3. Pressure versus displacement curves of the tests.

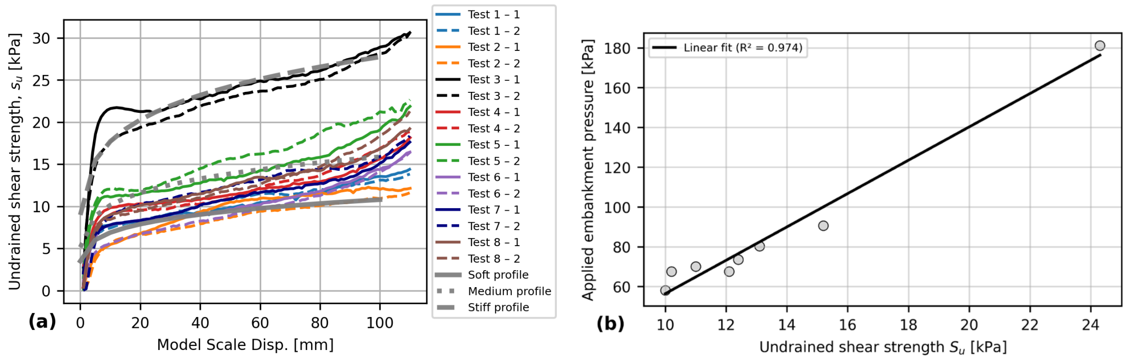

Figure 4. (a) Undrained shear strength profiles measured from in-flight T-bar penetration tests together with the analytical SHANSEP prediction; (b) scatter plot of embankment resistance as a function of the undrained shear strength at mid-depth of the foundation clay.

Table 1. Properties of the tests along with basic results.

Test ID	Ditch (Y/N)	Embankment D_r (%)	s_u at Reference Depth*	Peak Embank. Resistance (kPa)	Shear Rate (mm/s)
1	Y	87.2	11.0	69.9	0.2
2	N	77.5	10.2	67.5	0.2
3	Y	77.5	24.2	181.5	0.2
4	Y	81.1	12.1	67.4	0.2 / 2
5	Y	93.5	15.2	84.11	0.2 / 0.02
6	Y	96.3	9.9	57.9	0.2
7	Y	74.1	12.3	73.7	0.2
8	Y	80.8	12.5	NA (44.1**)	0.2

*Reference depth refers to the mid-depth of the clay profile

**Test 8 does not show a distinct peak, the selected value is at 100 mm prototype scale displacement (for indicative comparisons)

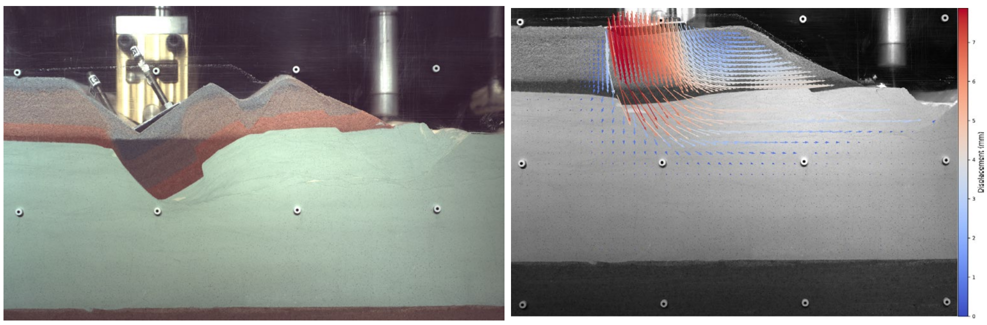

Figure 5. Exemplar images pertaining to Test 5: (a) failure geometry at the end of the test and (b) vector field of displacements at a prototype scale displacement level of 500 mm.

4 Deformation mechanisms and pore pressure evolution

Figure 6 illustrates the engineering shear strain values obtained in Test 5. The analysis method involved the use of GeoPIV-RG code [4]. The results reveal the progressive localization of shear strains beneath the embankment toe and within the upper portion of the clay foundation. At early stages of loading, deformation is concentrated beneath the loading plate, which corresponds to a punching-type mechanism. With increasing displacement, the shear strain field expands laterally and downward, forming a broader wedge-type failure mechanism. Figure 7 illustrates the relationship between the calculated strains and increment of pore water pressures due to loading at two select locations for PPT 8 and PPT 9 sensors (with the assumption that the strains seen on the transparent wall are projected to the backwall where the sensors are as per plane-strain assumption).

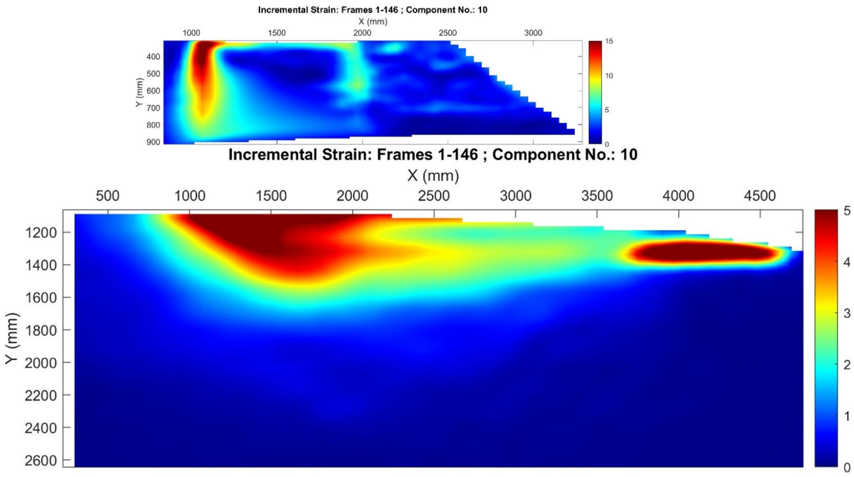

Figure 6. Shear strain plots of the exemplar test (Test 5).

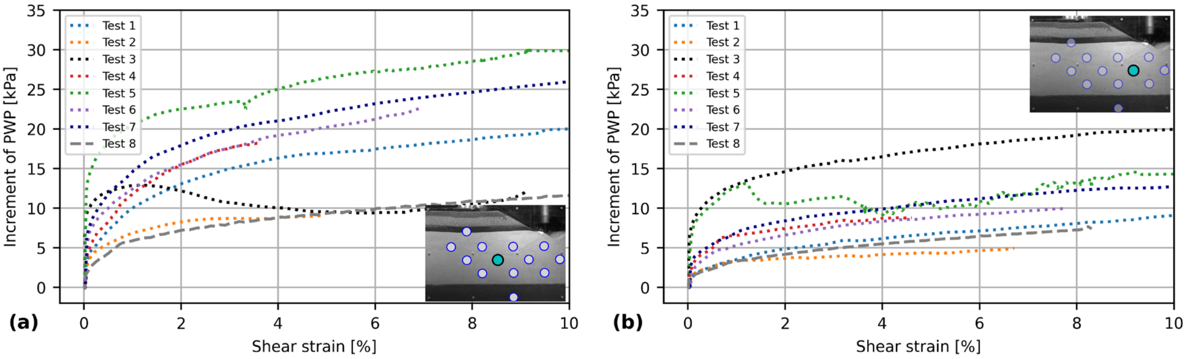

Figure 7. Increment of pore water pressure versus shear strains for pore water pressure sensor PPT 8 and 9 (here incremental refers to the pore water pressure developing with the onset of loading).

5 Conclusions

The centrifuge experiments conducted within the RESET research programme provide a controlled experimental dataset describing the response of railway embankments founded on soft clay. Systematic variation of clay undrained shear strength, loading rate, and geometric boundary conditions enabled isolation of the primary parameters governing embankment resistance and deformation.

The results indicate a clear relationship between foundation strength and peak embankment resistance. Full-field PIV measurements reveal progressive strain localisation within the clay foundation, which evolves from an initial punching-type response beneath the loading plate to a broader wedge-type failure mechanism accompanied by pore pressure development under undrained conditions.

References

1. C. Cengiz, T. Schweckendiek, A. van Uitert, C. Zwanenburg, Centrifuge modelling of railway embankments on soft clay: load-displacement behaviour, pore pressure development, and deformation mechanisms. Transp. Geotech. (under review)

2. C. Cengiz, T. Schweckendiek, A. van Uitert, C. Zwanenburg, Centrifuge modelling of railway embankments on soft clay: experimental observations from the RESET programme, in Proceedings of the ICPMG-2026 conference, Zurich, Switzerland, June 8-12 (to be published)

3. D. White, C. Gaudin, N. Boylan, H. Zhou, Interpretation of T-bar penetrometer tests at shallow embedment and in very soft soils. Can. Geotech. J. **47**, 218-229 (2010). https://doi.org/10.1139/T09-096

4. S.A. Stanier, J. Blaber, W.A. Take, and D.J. White, Improved image-based deformation measurement for geotechnical applications. Can. Geotech. J., **53**(5), 727-739 (2017). https://doi.org/10.1139/cgj-2015-0253@cgj-ec.2015.01.issue-5